Article:

eprints@whiterose.ac.uk
https://eprints.whiterose.ac.uk/

1   # Structural evolution of an alkali sulfate activated slag cement

2

3   Neda Mobasher, Susan A. Bernal and John L. Provis[*]

4

5   Immobilisation Science Laboratory, Department of Materials Science & Engineering,

6   The University of Sheffield, Sheffield S1 3JD, United Kingdom

7

8   * To whom correspondence should be addressed. Email j.provis@sheffield.ac.uk,

9   phone +44 114 222 5490, fax +44 114 222 5493

10

11   ## Abstract

12   In this study, the effect of sodium sulfate content and curing duration (from fresh paste up to

13   18 months) on the binder structure of sodium sulfate activated slag cements was evaluated.

14   Isothermal calorimetry results showed an induction period spanning the first three days after

15   mixing, followed by an acceleration-deceleration peak corresponding to the formation of bulk

16   reaction products. Ettringite, a calcium aluminium silicate hydrate (C-A-S-H) phase, and a

17   hydrotalcite-like Mg-Al layered double hydroxide have been identified as the main reaction

18   products, independent of the Na_2SO_4 dose. No changes in the phase assemblage were detected

19   in the samples with curing from 1 month up to 18 months, indicating a stable binder structure.

20   The most significant changes upon curing at advanced ages observed were growth of the AFt

21   phase and an increase in silicate chain length in the C-A-S-H, resulting in higher strength.

22

23   **Keywords:** Alkali-activated slag, sodium sulfate, microstructure, X-ray diffraction, nuclear

24   magnetic resonance spectroscopy

25

26

27   ## 1. Introduction

28

29   Ground granulated blast furnace slag, a by-product of the iron making industry, is one of the

30   main supplementary cementitious materials used in blends for partial replacement of Portland

31   cement. However, the amount of slag that can be incorporated in a Portland blended cement is

32   limited by the slower hydration of the slag, which delays the hardening of these cements.

33   Therefore, in the production of cements solely based on slag without a Portland cement

34 component, chemical activation is required to initiate the reactions that will lead to the

35 hardening of the material. In general, alkali silicates, hydroxides or their combination are used

36 as alkaline solutions for the activation process of slag, which are referred to as activating

37 solutions [1].

38

39 Alkali metal silicates and hydroxides cannot be naturally sourced, and their production process

40 is costly and energy-consuming, meaning that they have been identified as the dominant

41 contributor to the environmental footprint and production cost of alkali-activated cements [2].

42 However, these are not the only activators that can be used for the production of these binders.

43 One of the promising environmentally friendly alkali sources which can function as an activator

44 is sodium sulfate (Na_2SO_4), which is naturally found as thenardite (anhydrous Na_2SO_4) and

45 mirabilite ($Na_2SO_4 \cdot 10H_2O$) [3]. Activation of slag by near neutral salts has been given

46 relatively less consideration than silicate or hydroxide activation, as their utilisation

47 compromises the early strength development of these binders, and even the initial hardening of

48 the cement can take several days or longer [4].

49

50 Even though the strength development of Na_2SO_4 activated slag cement can be optimised and

51 improved to fit the needs of the construction industry, for some specialised applications, rapid

52 setting is not considered a key factor controlling the application of a cementitious system. For

53 instance, Na_2SO_4 activated slag has been evaluated as a potential matrix for the disposal of low

54 and intermediate level nuclear waste for its low heat of reaction and moderate pH, which is

55 proposed to be beneficial in reducing corrosion of radioactive metals [5]. It has also been

56 reported [6, 7] that immobilisation of sodium sulfate-bearing nuclear wastes is achievable in

57 $Ba(OH)_2$/Na_2SO_4-activated slag cements, where a process of combined sulfate/hydroxide

58 activation of the slag takes place, along with the precipitation of insoluble barium sulfate.

59

60 It is also worth noting that despite the delayed early reaction reported in these systems, it has

61 been identified [1] that Na_2SO_4-activated slag can develop mechanical strengths at 28 days

62 which are comparable to those identified in cements with higher early strength, such as NaOH-

63 activated slags. Recent studies have also shown [8] that Na_2SO_4-activated slags are more

64 resistant to degradation caused by exposure to elevated temperatures up to 600°C, in

65 comparison to Portland cement.

66

67 In sodium sulfate activation of slag, the main strength-giving phase forming is a calcium-
68 silicate-hydrate (C-S-H) type phase with a low Ca/Si ratio and a significant degree of
69 aluminium substitution, referred to as C-A-S-H [7]. As the main secondary reaction product,
70 ettringite ($3CaO \cdot Al_2O_3 \cdot 3CaSO_4 \cdot 32H_2O$) has been identified [7, 8]. This is associated with the
71 high sulfate content in these systems, which stabilises ettringite even at high alkalinity [9].
72 Formation of ettringite is considered to be desirable for nuclear waste encapsulation via
73 cementation, as its large unit cell accommodates a high content of bound water, leaving less
74 free water in the pore network available for radiolysis [10]. Radiolysis of free water
75 compromises the integrity of a solid cement wasteform as it causes formation of cracks and
76 open pores [11]. Ettringite can also act as a host for a number of both positively and negatively
77 charged ions in both the columnar and channel sections, as isomorphous substituents within its
78 structure [12]. This mechanism can be beneficial for encapsulation of hazardous wastes such
79 as heavy metals [13, 14], and also for many potentially problematic radionuclides.
80
81 This study focuses on the characterisation of the Na_2SO_4 activated slag cement system, with a
82 view towards developing a cement with potential for nuclear waste immobilisation. The effect
83 of different alkali concentrations on the reaction kinetics and phase assemblage has been
84 investigated. Microstructural evolution has been followed over 18 months via X-ray
85 diffraction, thermogravimetry, solid state nuclear magnetic resonance spectroscopy, scanning
86 electron microscopy and compressive strength development.
87
88

2. Experimental methods

90

2.1. Materials

92 A blast furnace slag (BFS) from Redcar steelworks, UK, with a Blaine fineness of 286 m^2/kg,
93 was used in this study. The chemical composition of the BFS is presented in Table 1. As alkali-
94 activator an analytical grade anhydrous sodium sulfate (Na_2SO_4, 99% purity) from Alfa Aesar
95 was used.
96
97
98

99   **Table 1.** Composition of blast furnace slag (BFS), from X-ray fluorescence analysis. LOI is loss on
100   ignition at 1000°C

Component as oxides	CaO	SiO$_2$	Al$_2$O$_3$	Fe$_2$O$_3$	MgO	K$_2$O	Na$_2$O	SO$_3$	others	LOI
Weight %	38.8	35.8	13.4	0.9	7.6	0.4	0.3	0.7	1.5	0.9

101

102

2.2.   Sample formulation and testing

104

105   Activating solutions containing 5, 10 and 25 wt.% Na$_2$SO$_4$ (i.e. 50, 100 and 250 g Na$_2$SO$_4$ per

106   kg of water) were prepared by dissolving solid anhydrous Na$_2$SO$_4$ in distilled water at 40°C.

107   The solutions were cooled to room temperature, were mixed with unreacted BFS, according to

108   the formulations given in Table 2. The pastes were weighed and combined in a sealed 50 mL

109   centrifuge tube, manually mixed and shaken for 2 to 5 minutes, then mechanically mixed for a

110   further 5 minutes using a Whirh Mixer. The samples were cured in the same sealed centrifuge

111   tubes at room temperature (21°C) for up to 18 months.

112

113   **Table 2.** Formulations for sodium sulfate activated slag samples

Sample ID	BFS (g)	Na$_2$SO$_4$ (g)	H$_2$O (g)	Water/binder ratio*	Activator dose (g Na$_2$O per 100 g of BFS)
5 wt.%	100	1.8	35	0.34	0.79
10 wt.%	100	3.9	35	0.34	1.70
25 wt.%	100	11.7	35	0.31	5.11

114   * water/binder ratio was calculated considering the sum of Na$_2$SO$_4$ + BFS to be the binder

115

116   In the context of encapsulation/immobilisation of nuclear wastes, the workability of the cement

117   wasteform material is very important, as this will control its ability to fill the complex shape of

118   the drums used for nuclear waste treatment in the UK, without requiring additional vibration.

119   All the pastes produced in this study were highly fluid during the mixing and casting process,

120   and did not harden within the first 24h after mixing.

121

122 In order to elucidate when the pastes did harden, isothermal calorimetry experiments were

123 conducted using a TAM Air isothermal calorimeter at a base temperature of 25°C ± 0.02°C.

124 Fresh paste was mixed externally as described above, 25 g was weighed into an ampoule and

125 immediately placed in the calorimeter, and the heat flow was recorded for the first 400 h of

126 reaction. All values of heat release rate are normalised by total mass of paste.

127

128 ## 2.3 Tests and analysis

129

130 Hardened pastes were demoulded after different times of curing, cut into cylinders (27 mm

131 diameter and 27 mm height) for compressive strength testing, and the ends polished to be flat

132 and parallel. After testing to failure in compression, the broken pieces were immersed in

133 acetone to arrest the reaction process. After 3 days, the samples were removed from the acetone,

134 dried, and kept in sealed containers to avoid carbonation during storage. The samples were then

135 crushed and sieved (-63 μm), and analysed:

136 - X-ray diffraction (XRD) was conducted using a Siemens D5000 instrument (Cu $K_{\alpha1}$, λ

137   = 1.54178 Å), with a step size of 0.02° and a scanning speed of 0.5°/min.

138 - Thermogravimetric analysis (TGA) was carried out using a Perkin Elmer Pyris 1 TGA.

139   Approximately 40 mg of sample was weighed, placed and heated at 10°C/min in an

140   alumina crucible under a nitrogen atmosphere.

141 - Solid-state ^{29}Si MAS NMR spectra were collected at 59.56 MHz on a Varian Unity

142   Inova 300 (7.05 T) spectrometer using a probe for 7.5 mm o.d. zirconia rotors and a

143   spinning speed of 5 kHz. The ^{29}Si MAS NMR employed a 90° pulse duration of 5 μs,

144   a relaxation delay of 5 s, and 14,000 scans. Solid-state ^{27}Al MAS NMR spectra were

145   acquired at 104.198 MHz, using a Varian VNMRS 400 (9.4T) spectrometer and a probe

146   for 4 mm o.d. zirconia rotors, a spinning speed of 14 kHz with a pulse width of 1 μs

147   (approximately 25°), a relaxation delay of 0.2 s, and a minimum of 7000 scans. ^{29}Si and

148   ^{27}Al chemical shifts are referenced to external samples of tetramethylsilane (TMS) and

149   a 1.0 M aqueous solution of $Al(NO_3)_3$, respectively.

150 - Environmental scanning electron microscopy (SEM) was conducted using a Hitachi

151   TM3030 microscope, with a backscattered electron detector and an accelerating voltage

152   of 15 keV. Monolithic solid samples were cut into small pieces with a diamond saw

153   before sanding manually with grinding papers of 400, 800 and 1200 grit SiC. Samples

154   were then polished with 6 μm, 3 μm, 1 μm and 0.25 μm diamond pastes and polishing

155 cloths. The samples were finally coated with carbon using an Edwards 'speedivac'
156 carbon coating unit and silver dagged to make them electrically conductive before
157 analysis.

158 • Compressive strength of cylindrical specimens was measured using a Zwick Roell
159 Z050 machine at a load rate of 0.5 mm/min. The results were corrected using a shape
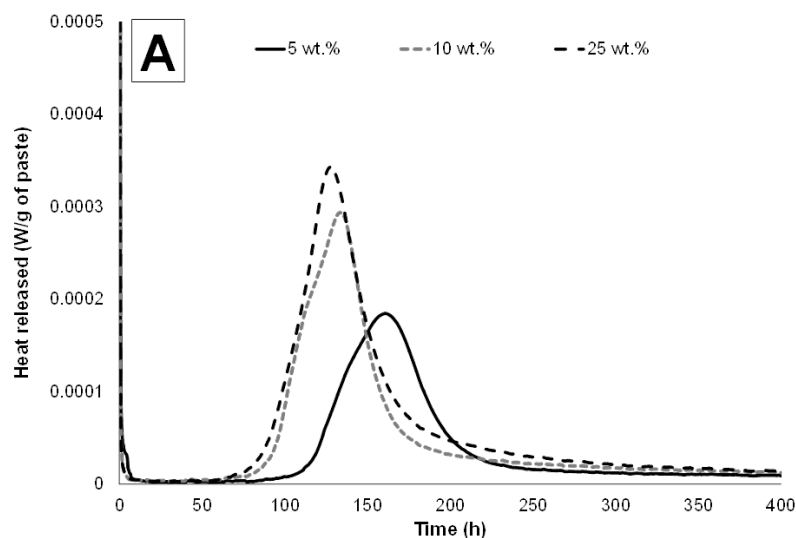160 factor of 0.85 for cylinders of aspect ratio 1.0.

161

162

163 ## 3. Results and discussion

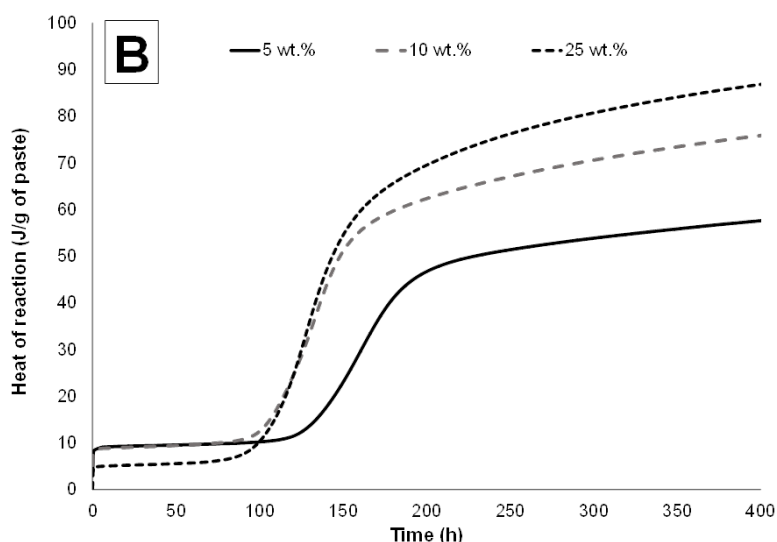164 ## 3.1. Effect of the activator concentration

165 ### 3.1.1. Isothermal calorimetry

166 Figure 1 shows the heat release curves of alkali sulfate activated slag binders, as a function of
167 the Na_2SO_4 solution concentrations. In general, all curve shapes are consistent with the
168 previous results reported for alkali activated slag systems with hydroxide and silicate
169 activators, where a pre-induction period (first peak) is observed during the first hours of
170 reaction, followed by an induction period, and a high intensity acceleration and deceleration
171 period (second peak), corresponding to the initial and final setting of the paste as a consequence
172 of the precipitation of reaction products [15-17].

173

174

175

Figure 1. (A) Isothermal calorimetry curves and (B) cumulative heats of reaction of alkali
sulfate activated slag binders, as a function of the Na_2SO_4 concentration.

The main distinction for Na_2SO_4 activated slag pastes compared to the calorimetry curves identified for alkali silicate and hydroxide activated slag systems, is the very long induction period (between 100-125 hours) observed here before the precipitation of reaction products starts taking place. This can be attributed to the near-neutral pH of the alkali activator solutions used (pH~7.5), which does not greatly accelerate the dissolution of the slag particles. The results reported here are comparable with those reported by Rashad et al. [18] for Na_2SO_4 activation of slag, where induction periods between 24 to 60 hours were identified at a reaction temperature of 40°C, depending on the fineness of the slag and the activator dose.

Figure 1B shows that the duration of the induction period is nearly comparable for all the samples, but an increased concentration of the activator is not promoting a faster reaction of the slag, as might be expected. Instead, the use of 10 wt.% and 25 wt.% Na_2SO_4 solutions gave comparable induction periods (~80 h), while 5 wt.% gave a longer induction period of ~110 h.

Fig. 1B also shows that the 25 wt.% Na_2SO_4 activated slag sample has the highest overall heat release after 400 hours of reaction, whereas the 5 wt.% Na_2SO_4 activated slag sample has a broad and low intensity acceleration-deceleration period, nearly 50% lower in overall heat of reaction compared with the 25wt.% Na_2SO_4 sample.

198   These results elucidate that in the range of activator doses evaluated in this study, the duration

199   of the induction period of Na_2SO_4 activated slag samples does not have a direct correlation

200   with the alkali solution concentrations; however, slightly higher cumulative heats of reaction

201   are observed at extended times of reaction when the alkali solution concentrations   are

202   increased, consistent with the observation of Rashad et al. [18]. Therefore, a high concentration

203   of the activator can induce higher degrees of reaction, but not necessarily the fastest initiation

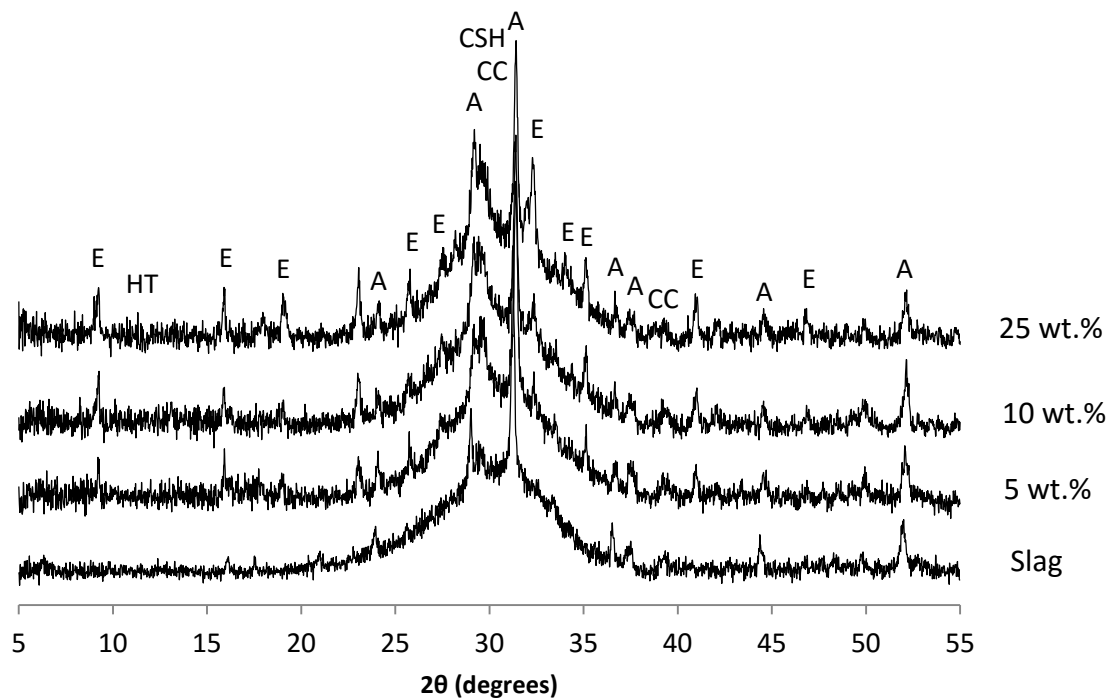204   of the formation of bulk reaction products.

205

206

3.1.2. X-ray diffraction

208   Figure 2 illustrates X-ray diffractograms of Na_2SO_4-activated slag pastes with various sodium

209   sulfate solution concentrations, after 28 days of curing at 21°C. Åkermanite ($Ca_2MgSi_2O_7$,

210   Powder Diffraction File, PDF, card #076-0841), is identified as the sole crystalline present in

211   the slag used in this study, and the reflections assigned to this phase are still observed in the

212   activated binders, which suggest that it is not participating in the activation reaction

213

214   All the samples show formation of ettringite ($3CaO \cdot Al_2O_3 \cdot 3CaSO_4 \cdot 32H_2O$; PDF # 041-1451),

215   in agreement with previous reports for similar systems [5, 19]. The ettringite peak intensity

216   increased with higher sulfate content within the system, consistent with the higher degree of

217   reaction identified by calorimetry (Figure 1B) with higher contents of sodium sulfate in the

218   system. A low intensity peak at 11.3° 2θ is also observed in these samples, and is assigned to

219   a layered double hydroxide type phase (LDH). In alkali-activated slags with moderate to high

220   MgO contents, such layered double hydroxides are usually identified as hydrotalcite

221   $Mg_6Al_2(CO_3)(OH)_{16} \cdot 4H_2O$ [17] or variants thereof; however, under the activation conditions

222   adopted in this study, the formation of hydroxyl or sulfate rich LDH might be feasible. XRD

223   reflections for sulfate-rich LDH were checked, however the main peaks of this type of phase

224   overlaps with those assigned to ettringite, so it cannot be stated conclusively from the XRD

225   results whether the formation of this phase is taking place.

226

227

228 **Figure 2**. X-ray diffractograms of one month Na_2SO_4-activated BFS pastes with various

229 sodium sulfate solution concentrations. Peaks marked are åkermanite (A), calcite (CC),

230 ettringite (E), hydrotalcite (HT) and C-A-S-H (CSH)

231

232 Despite the high Na_2SO_4 doses used in this study, unreacted Na_2SO_4 in the forms of mirabilite

233 and thenardite was not identified as a crystalline products in these samples, nor was gypsum

234 formation observed. This indicates that the majority of the sulfate has reacted to form ettringite,

235 and that sufficient Ca and Al have been released by the slag to enable this conversion to be

236 completed, even at the highest dose (25 wt.% solution corresponding to 11.7 g Na_2SO_4 per 100

237 g slag, Table 2). In a previous study by the authors [7], traces of unreacted Na_2SO_4 were

238 identified via ^{23}Na MAS NMR spectroscopy in a mix design corresponding to the 10wt.%

239 Na_2SO_4 samples studied here, after 6 months of curing. Therefore it is likely that the Na_2SO_4

240 was not sufficiently crystalline to be identified by XRD, but is also possible that some of the

241 unreacted Na_2SO_4 was removed during the sample preparation prior testing.
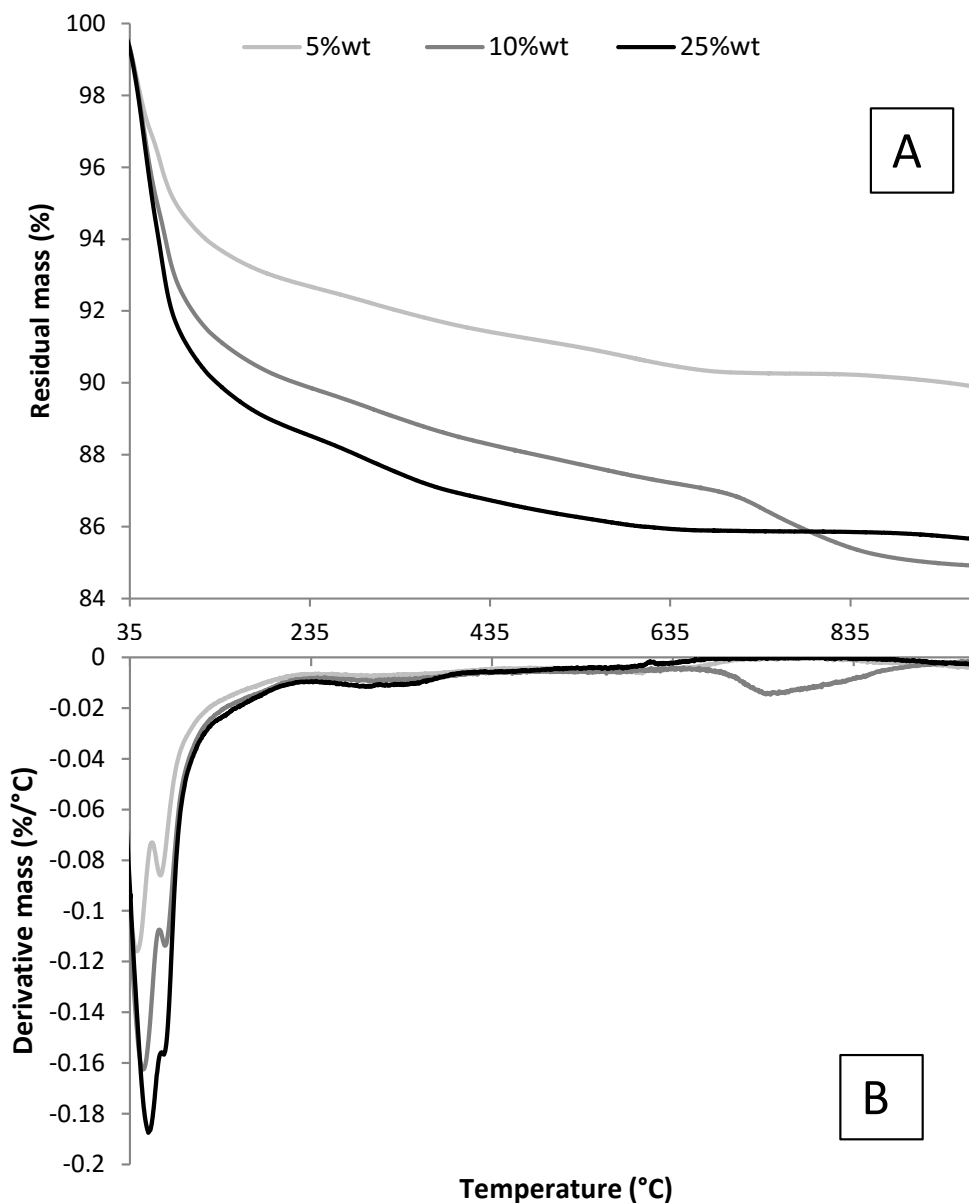
242

243 Disordered calcium silicate hydrate (C-S-H) type gel products are also identified in all samples

244 as a very broad reflection centred below 30° 2θ. This type of product is the main binding phase

245 in alkali-activated slag systems [20], and appears to increase in prevalence (concentration

246 and/or crystallinity) with increasing activator dose, consistent with the higher heat release at

247 the highest activator content tested. Traces of calcite are also identified in these samples, which

248 is likely to be associated with weathering of the sample prior to analysis.

249

3.1.3. Thermogravimetric analysis (TGA)

251 The differential thermograms (DTG) of Na_2SO_4-activated slag samples with various

252 concentration of the activator are shown in Figure 3. The slightly higher weight loss of the

253 sample with 10wt.% Na_2SO_4, compared with the paste dosed with a higher Na_2SO_4 content, is

254 mainly associated with the thermal decomposition of calcite, which was identified in these

255 samples by XRD (Figure 2), and whose decomposition takes place between 650°C to 850°C

256 [21].

257

258 **Figure 3.** Thermograms (A) and differential thermograms (mass loss downwards) (B) of

259 Na₂O₄-activated slag pastes cured for 28 days, with various sodium sulfate solution

260 concentrations

261

262 A high intensity mass loss between 70°C and 200°C is observed for all the samples, attributed

263 to the release of evaporable water and the start of the dehydration of ettringite [22]. The total

264 mass loss up to 200°C increases from 7.1% for the sample activated with 5 wt.% Na_2SO_4 to

265 11.1% with 25 wt.% Na_2SO_4 respectively, indicating that a higher concentration of the activator

266 promotes the formation of a larger amount of reaction products, consistent with the escalation

267 of ettringite formation as observed in the XRD results (Figure 2). The progressive weight loss

268 between 30°C and 200°C is assigned to the decomposition of the C-S-H type phase [23]

269 forming in these samples.

270

271 The weight loss between 200°C and 400°C is assigned to decomposition of the layered double

272 hydroxide (LDH) with a hydrotalcite-like structure [24]. Comparable weight losses assigned

273 to LDH decomposition were observed in all samples, independent of the concentration of

274 activator used, which is consistent with the fact that most of the aluminium is being consumed

275 during the ettringite formation.

276

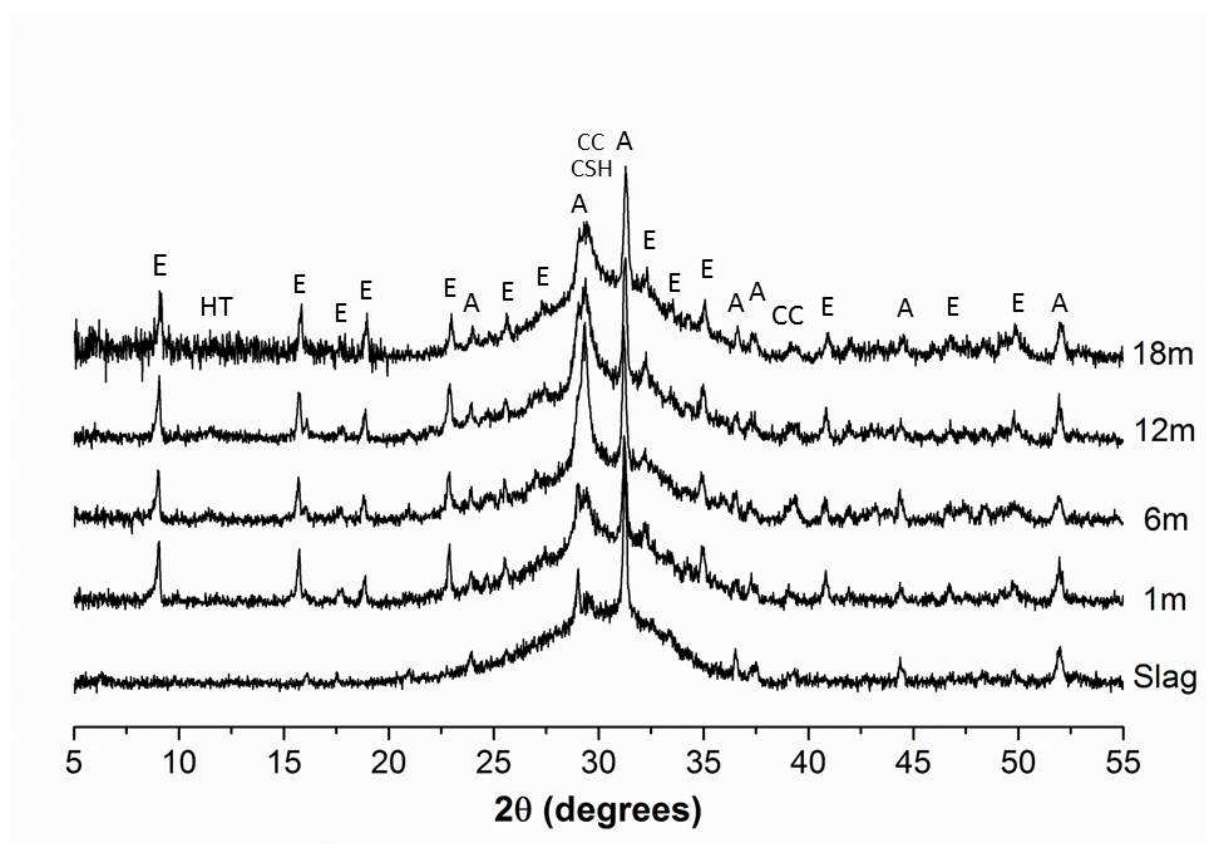277 ## 3.2. Effect of curing duration

278 Pastes produced with 10 wt.% Na_2SO_4 were selected for the assessment of the structural

279 evolution of sodium sulfate activated slag pastes.

280

281 ### 3.2.1. X-ray diffraction

282 Ettringite, a hydrotalcite-like LDH type phase, traces of calcium carbonate and a disordered C-

283 A-S-H were identified at all ages (Figure 4), consistent with observations at 28 days (Figure

284 2). No significant changes in the intensity of the reflections of the crystalline phases forming

285 were observed during this 18 month period. The most notable change in the diffractograms is

286 observed in the region assigned to the overlapping reflections of C-A-S-H and calcite, where

287 this peak seems sharper and more intense up to 6 months, and afterwards become less intense

288 and wider. The secondary peak of calcite just below 40° 2θ shows a very similar trend,

289 indicating that this change is due largely to the differences in superficial carbonation of the

290 samples, where the more mature 12- and 18-month samples are less prone to carbonation prior

291 to or during analysis, although there may also be some changes in the content or ordering of
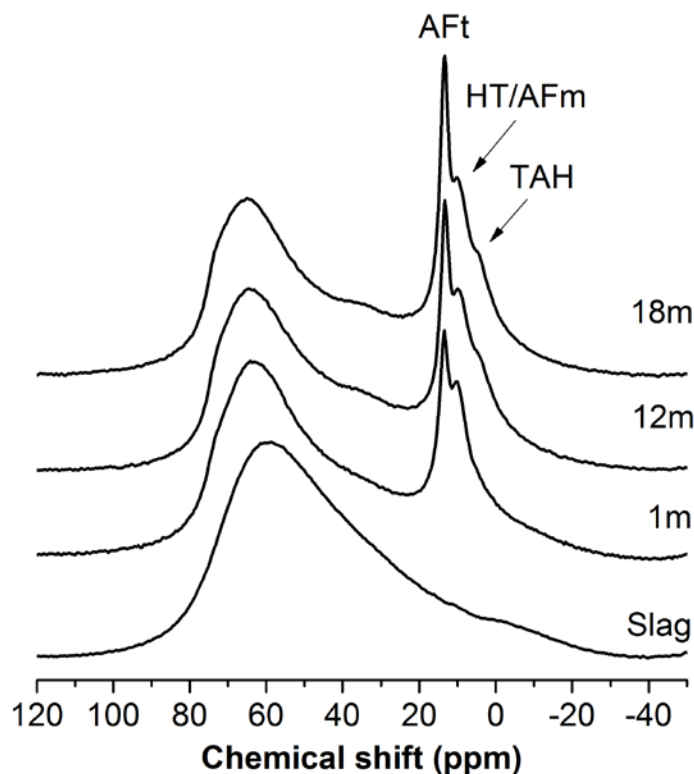292 the C-A-S-H as a function of time.

293

294 **Figure 4.** X-ray diffractograms of unreacted slag and Na_2SO_4-activated slag pastes with
295 various ages in months as marked. Peaks marked are åkermanite (A), calcite (CC), ettringite
296 (E), hydrotalcite (HT) and C-S-H (CSH)

297

3.2.2. Solid-state ^{27}Al MAS NMR spectroscopy

299 The ^{27}Al MAS NMR spectra of the samples (Figure 5) show three distinct Al coordination
300 environments (Al^{IV}, Al^V and Al^{VI}), located at chemical shifts between 52 to 80 ppm, 30 to 40
301 ppm and -10 to 15 ppm, respectively [25]. In the spectrum of the unreacted slag, a broad
302 asymmetric Al^{IV} band centred at 60 ppm is observed, and assigned to the aluminosilicate glassy
303 fraction of the slag resembling a melilite type structure [25]. Upon sodium sulfate activation of
304 the slag, new resonances in the Al^{VI} region, centred at 13 ppm, 10 ppm and 4 ppm were
305 identified. These resonances are assigned to ettringite [26], and to the hydrotalcite type phase
306 [20], respectively, as both of these phases were observed by XRD (Figure 4). The contribution
307 of ettringite increases with the time of curing. Minor contributions from AFm type phases could
308 also potentially be assigned to the band at 10 ppm, although such phases were not identifiable

309   by XRD or TGA in the samples studied here. The low intensity band centred at 4 ppm, mainly

310   observed after 12 and 18 months of curing, is attributed to the third aluminate hydrate (TAH)

311   [27], as this phase has been identified in other alkali-activated slag systems [28].

312

Figure 5. ^{27}Al MAS NMR spectra of unreacted slag and Na2SO4-activated slag pastes with various ages. AFt corresponds to ettringite, HT corresponds to hydrotalcite and TAH corresponds to the third aluminate hydrate

316

317   The increase in intensity in the Al^V region, particularly from 1 month to 12 months of curing,

318   is related to the incorporation of 5-coordinated Al into the interlayer sites in C-A-S-H structures

319   [27]. The aluminium environments in the Al^{IV} region correspond in part to the remnant

320   unreacted slag in the binders, and to the C-A-S-H gel forming upon activation of the slag. C-

321   A-S-H gels usually present three distinctive sites centred at 73 ppm, 67 ppm and 62 ppm,

322   respectively [29-31]. The sites at 73 and 67 ppm may be assigned to the q^2 aluminate species

323    $q^2(I)$ and $q^2(II)$ in the gel as bridging tetrahedral sites coordinated with different cationic

324   interlayer species [28], analogously with the $Q^1(I)$ and $Q^1(II)$ silicate sites identified in silicate-

325   activated slag binders [17, 28]. The sites at 62 ppm are assigned to q^3 coordinated aluminium,

326   associated with a high degree of crosslinking in the C-A-S-H gel [28].
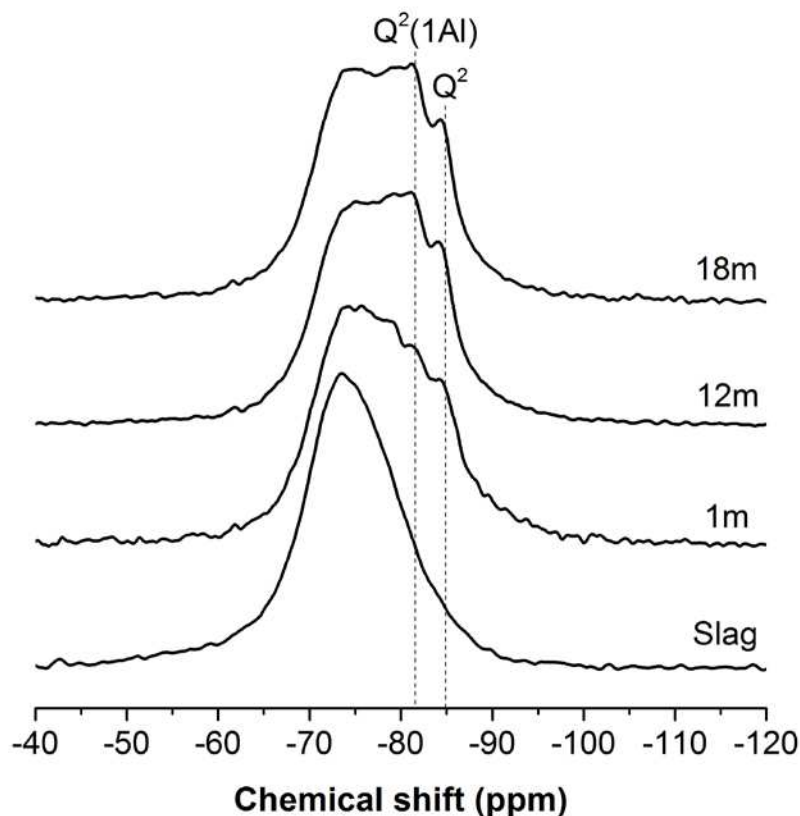
327

328   In the one month old sample the asymmetric Al^{IV} band is centred at 60 ppm, indicating either

329   a large degree of cross-linking of the C-A-S-H forming in this paste, or more likely the presence

330   of a large fraction of unreacted slag remaining in the sample. At advanced times of curing, this

331   band is less intense and shifted towards higher chemical shift values (64 and 65 ppm,

332   respectively) compared with the one-month sample. This is associated with the consumption

333   of the slag as reaction progresses over the time of curing.

334

3.2.3. Solid-state ^{29}Si MAS NMR spectroscopy

336   Figure 6 shows the ^{29}Si MAS NMR spectra of the unreacted slag used, and of 10 wt.% Na_2SO_4-

337   activated pastes with various ages. The unreacted slag spectrum has a line shape comparable

338   to the spectrum reported for åkermanite [20], which is identified as the main crystalline phase

339   in the slag used in this study (Figure 2) , with a resonance centred at -74 ppm. A reduction of

340   the intensity of this band is associated with the progressive reaction of the slag over the time

341   of curing. In the sulfate-activated samples, resonances between -80 ppm and -90 ppm are

342   observed, consistent with the formation of a C-A-S-H type phase as previously demonstrated

343   by ^{27}Al MAS NMR (Figure 5). In particular, resonances between -82 ppm and -85 ppm in

344   Figure 6, corresponding to Q^2(1Al) and Q^2 sites respectively, are assigned to Al-substituted C-

345   S-H type gel with a tobermorite type structure [27, 32]. The intensities of the Q^2(1Al) and Q^2

346   sites increase significantly after 12 and 18 months of curing, compared with the one month

347   sample. This is consistent with the formation of more C-A-S-H in the system as reaction

348   progresses, as identified in the ^{27}Al MAS NMR results (Figure 5). Resonances in the region -

349   78 to -80 ppm in Figure 6 are assigned to Q^1 sites in the C-A-S-H type gel, however they

350   overlap with the signal corresponding to the unreacted slag, therefore it is difficult to identify

351   any trends regarding this site without deconvolution of the spectra. Such deconvolution was

352   not carried out here, as it remains unknown whether the alkalinity conditions reached in sulfate

353   activated binders will be sufficient to promote congruent dissolution of the slag, and the

354   quantification of the different silicon sites can be influenced significantly if the slag dissolves

355   incongruently.

356

357

Figure 6. ^{29}Si MAS NMR spectra of unreacted slag and Na$_2$SO$_4$-activated slag pastes with various ages. Dashed lines indicate the position of Q^2(1Al) and Q^2 sites.
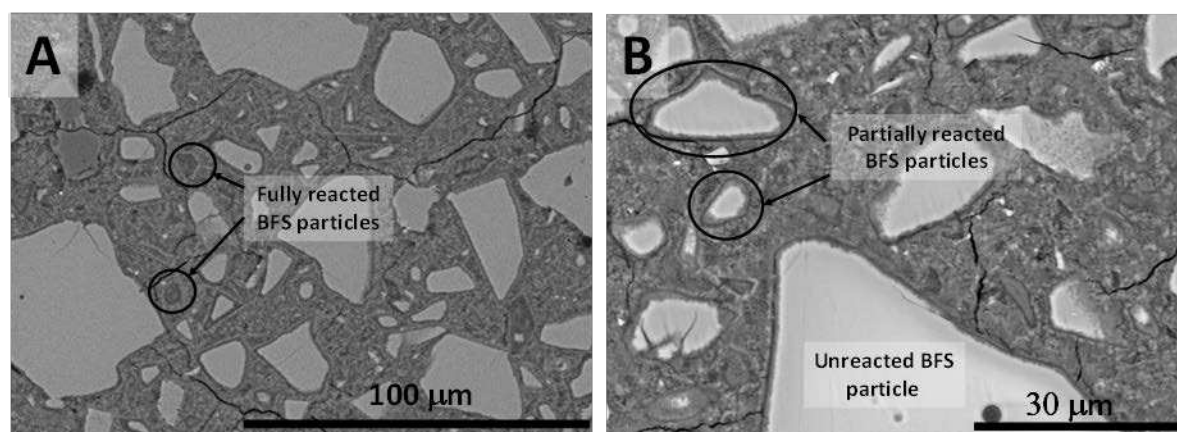
360

3.2.4. Scanning electron microscopy

Figure 7 shows backscattered electron (BSE) images of an 18-months cured 10 wt.% Na$_2$SO$_4$ activated slag paste, at different magnifications. In both images, light grey particles with angular morphology correspond to the unreacted slag. It is clearly identified that small slag particles are fully reacted, while the larger particles are partially reacted. The binding matrix seems to be dense and cohesive. In the higher magnification images (Fig. 7B), the formation of a dark rim of reaction products around the slag particles is observed, distinct from the main binding matrix. This indicates differences either in the chemical composition or density of the reaction products forming around the slag particles, compared to the main binding phase [33].

370

371

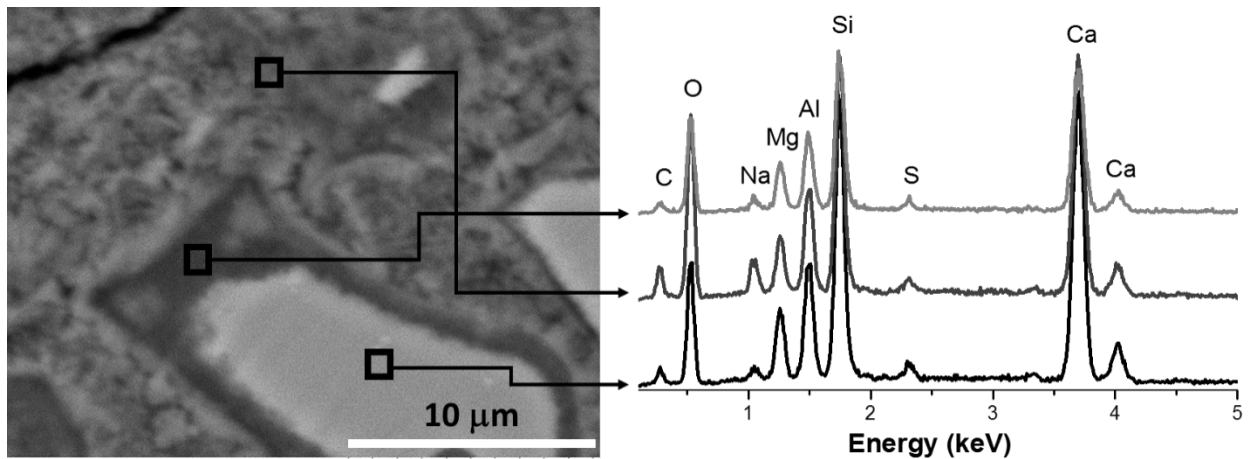**Figure 7.** Backscattered electron images of an 18-months cured 10 wt.% Na$_2$SO$_4$ activated slag paste with different magnifications.

Figure 8 shows a higher-magnification image of a partially reacted slag particle surrounded by a dark rim and main binding matrix. The chemical analysis results indicate that the unreacted slag particle, with a light grey colour, has a high concentration of calcium, silicon, magnesium and aluminium but low sulphur and sodium content compared with the other regions assessed. The main binding matrix, with a medium grey colour, has comparable chemical composition to the unreacted slag, but with additional S and Na corresponding to the contribution of the activator in this region, and with a lower overall density as this material is hydrous and porous. In the dark rim region, there is a significant decrease in the intensity of the calcium, silicon and aluminium bands, compared with the EDX spectrum of the main binding matrix, while the Mg concentrations are much more similar between the two regions.

These results are consistent with what has been identified in aged alkali-activated slag materials [34-36], where there are two distinct gel phases in the binder. The 'inner' gel is typically observed in the areas near surrounding unreacted slag particles, with a darker colour as a consequence of the lower density and reduced Ca/Si ratio of the C-A-S-H type gels, and with a higher content of Mg-rich phases. The 'outer' type gel forms further away from the slag particles and presents a lighter grey colour, which is associated with the higher Ca/Si ratio of the C-A-S-H type gel in this region. The formation of this multi-rim structure in aged activated slag binders has been compared with a Liesegang-type ring formation, where the reaction is believed to be following an Ostwald type super-saturation-nucleation-depletion cycle [36].
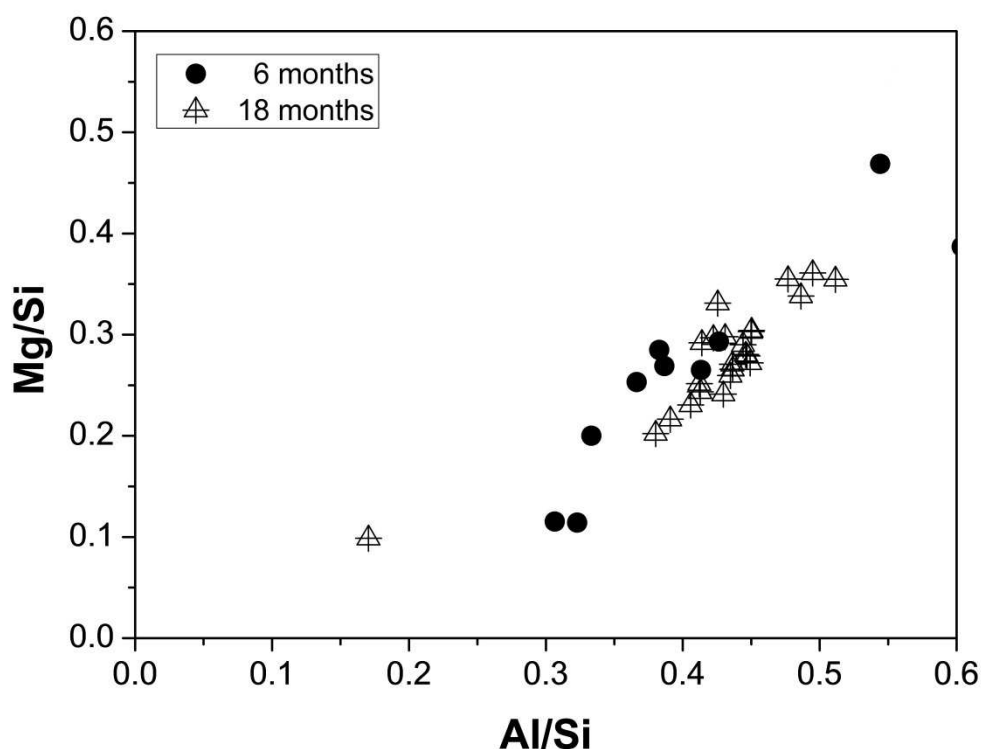
Figure 8. Backscattered electron image of an 18-months cured 10 wt.% Na_2SO_4 activated slag paste activated slag pastes, and EDX spectra of each of the regions identified in the micrograph

Figure 9 shows a plot of the atomic ratios Mg/Si vs Al/Si as determined by EDS spot analysis of 10 wt.% Na_2SO_4 activated slag pastes cured for 6 and 18 months. It has been reported that generally magnesium is incorporated in the hydrotalcite like LDH product that can also occur as a near micro-scale combination with C-S-H gel [37, 38]. It is clear from Figure 9 that in this case the atomic ratio Mg/Al is close to 2, which is representative of quintinite $Mg_4Al_2(OH)_{12}CO_3 \cdot H_2O$, another form of Mg–Al carbonate LDH and a member of the hydrotalcite group, rather than the 3:1 ratio of true hydrotalcite [39].
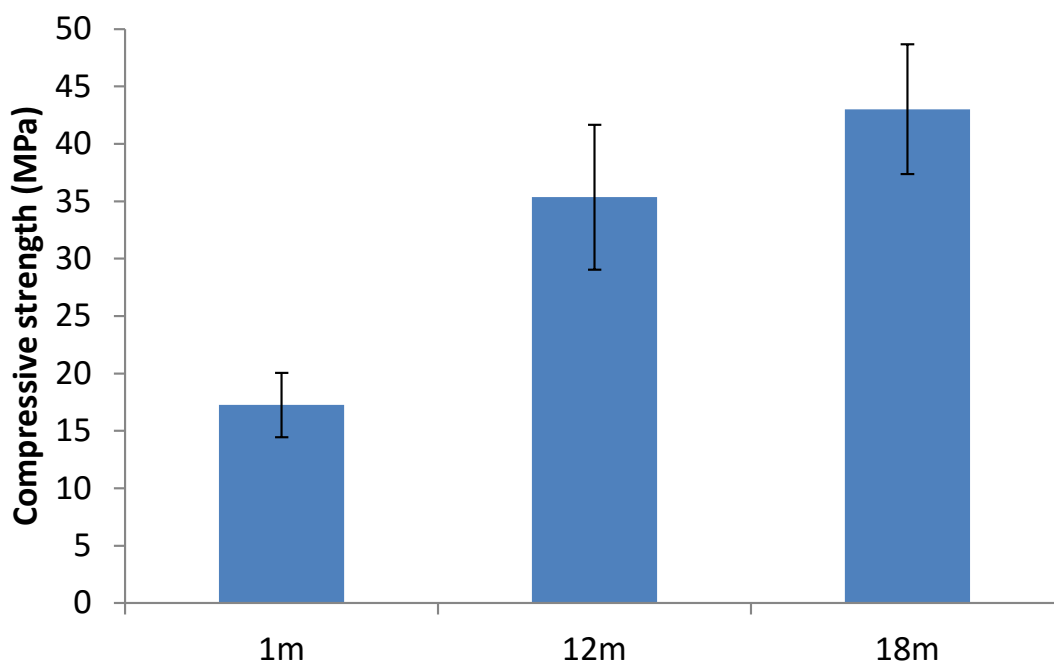
409

Figure 9. Atomic ratios Mg/Si vs Al/Si, in 10 wt.% Na_2SO_4 activated slag pastes cured for 6 and 18 months.

412

3.2.5. Compressive strength

The evolution of the compressive strength of the 10 wt.% Na_2SO_4 activated slag paste over the time of curing is shown in Figure 10. After one month of age the specimens showed a strength of 17 MPa, which is significantly lower than what can be obtained using sodium hydroxide or silicate activators as has been identified in other studies [40], but which is still entirely sufficient for waste immobilisation purposes where the strength requirements are not onerous. After 12 and 18 months of curing, these pastes develop compressive strengths of 35 MPa and 43 MPa respectively, and the ongoing strength development is consistent with the additional formation of C-A-S-H during extended curing as identified through the various analytical techniques applied in this paper.

423

Figure 10. Compressive strength of Na_2SO_4-activated slag pastes with various ages in months as indicated. Error bars show one standard deviation among three measurements

The continued strength development observed in the samples assessed here demonstrates that despite the delayed reaction taking place in these sulfate activated slag binders produced with a highly coarse slag, at advanced times of curing the reaction progresses, leading to a significant strength gain.

4.   Conclusions

Alkali sulfate activated slag cement has been assessed in terms of activator content and long term curing duration, up to 18 months. The results of isothermal calorimetry for various activator concentrations show that the dissolution and precipitation period can be delayed by up to 5 days at 25°C, but the binders do eventually set, harden and develop sufficient strength for utilisation as a waste immobilisation matrix. The induction period is not always reduced by an increase in activator dose or concentration, although more concentrated activating solutions do yield a higher extent of reaction.

X-ray diffraction and electron microscopic analysis of the 10 wt.% Na_2SO_4 formulation sample over an 18 month curing period demonstrates no changes in the nature of the crystalline phases (ettringite and a hydrotalcite-group phase with Mg/Al ~ 2) present, but the ^{29}Si and ^{27}Al MAS

446 NMR results verify that the formation of both C-A-S-H and ettringite is increased at extended

447 curing times, as the slag continues to react. These binders develop sufficient strength for waste

448 immobilisation applications, exceeding 15 MPa by 28 days and continuing to gain strength

449 with extended curing. However, considering the high contents of sulphates present in these

450 cementitious binders, determination of their dimensional stability over long periods of time is

451 required to assure the safe utilisation of these binders as potential alternatives for the

452 encapsulation/immobilisation of nuclear wastes.

453

5. Acknowledgements

6. References

466 1. Shi, C., P.V. Krivenko, and D.M. Roy, *Alkali-Activated Cements and Concretes*.
467   2006, Abingdon, UK: Taylor & Francis. 376 pp.
468 2. McLellan, B.C., et al., *Costs and carbon emissions for Geopolymer pastes in*
469   *comparison to Ordinary Portland Cement.* Journal of Cleaner Production, 2011. **19**(9-
470   10): p. 1080-1090.
471 3. Provis, J.L., et al., *Historical aspects and overview.* in: *Alkali Activated Materials,*
472   *State of the Art Report*, *RILEM TC 224-AAM*, J.L. Provis and J.S.J. van Deventer,
473   Editors. 2014: RILEM/Springer, Dordrecht. p. 11-57.
474 4. Bernal, S.A., Provis, J.L., Fernández-Jiménez, A., Krivenko, P.V., Kavalerova, E.,
475   Palacios, M. and Shi, C., *Binder chemistry – High-calcium alkali-activated materials*,
476   in: *Alkali Activated Materials, State of the Art Report*, *RILEM TC 224-AAM*, J.L.
477   Provis and J.S.J. van Deventer, Editors. 2014: RILEM/Springer, Dordrecht. pp. 59-91.
478 5. Bai, Y., et al., *The potential for using slags activated with near neutral salts as*
479   *immobilisation matrices for nuclear wastes containing reactive metals.* Journal of
480   Nuclear Materials, 2011. **413**(3): p. 183-192.
481 6. Mobasher, N., et al., *Ba(OH)$_2$ – blast furnace slag composite binders for the*
482   *encapsulation of sulphate bearing nuclear waste.* Advances in Applied Ceramics,
483   2014. **113**(8): p. 460-465.

7. Mobasher, N., et al., *Characterisation of Ba(OH)$_2$–Na$_2$SO$_4$-blast furnace slag cement-like composites for the immobilisation of sulphate bearing nuclear wastes.* Cement and Concrete Research, 2014. **66**: p. 64-74.

8. Rashad, A.M., et al., *Chemical and mechanical stability of sodium sulfate activated slag after exposure to elevated temperature.* Cement and Concrete Research, 2012. **42**(2): p. 333-343.

9. Clark, B.A. and P.W. Brown, *The formation of calcium sulfoaluminate hydrate compounds: Part I.* Cement and Concrete Research, 1999. **29**(12): p. 1943-1948.

10. Collier, N.C., et al., *The suitability of a supersulfated cement for nuclear waste immobilisation.* Journal of Nuclear Materials, 2014. **452**(1–3): p. 457-464.

11. Mobasher, N., et al., *Gamma irradiation resistance of an early age slag-blended cement matrix for nuclear waste encapsulation.* Journal of Materials Research, 2015. **30**(9): p. 1563-1571.

12. Gougar, M.L.D., B.E. Scheetz, and D.M. Roy, *Ettringite and C-S-H Portland cement phases for waste ion immobilization: A review.* Waste Management, 1996. **16**(4): p. 295-303.

13. Albino, V., et al., *Potential application of ettringite generating systems for hazardous waste stabilization.* Journal of Hazardous Materials, 1996. **51**(1–3): p. 241-252.

14. Kumarathasan, P., et al., *Oxyanion substituted ettringites: Synthesis and characterization; and their potential role in immobilization of As, B, Cr, Se and V.* Materials Research Society Symposium Proceedings, 1990. **178**: p. 83-104.

15. Fernández-Jiménez, A. and F. Puertas, *Alkali-activated slag cements: Kinetic studies.* Cement and Concrete Research, 1997. **27**(3): p. 359-368.

16. Ben Haha, M., et al., *Influence of slag chemistry on the hydration of alkali-activated blast-furnace slag -- Part I: Effect of MgO.* Cement and Concrete Research, 2011. **41**(9): p. 955-963.

17. Bernal, S.A., et al., *MgO content of slag controls phase evolution and structural changes induced by accelerated carbonation in alkali-activated binders.* Cement and Concrete Research, 2014. **57**: p. 33-43.

18. Rashad, A., et al., *Hydration and properties of sodium sulfate activated slag.* Cement and Concrete Composites, 2013. **37**: p. 20-29.

19. Gruskovnjak, A., et al., *Hydration mechanisms of super sulphated slag cement.* Cement and Concrete Research, 2008. **38**(7): p. 983-992.

20. Bernal, S.A., et al., *Gel nanostructure in alkali-activated binders based on slag and fly ash, and effects of accelerated carbonation.* Cement and Concrete Research, 2013. **53**: p. 127-144.

21. Maciejewski, M., H.-R. Oswald, and A. Reller, *Thermal transformations of vaterite and calcite.* Thermochimica Acta, 1994. **234**: p. 315-328.

22. Hall, C., et al., *Thermal decomposition of ettringite Ca$_6$[Al(OH)$_6$]$_2$(SO$_4$)$_3$.26H$_2$O.* Journal of the Chemical Society, Faraday Transactions, 1996. **92**(12): p. 2125-2129.

23. Myers, R.J., et al., *Effect of temperature and aluminium on calcium (alumino) silicate hydrate chemistry under equilibrium conditions.* Cement and Concrete Research, 2015. **68**: p. 83-93.

24. Kanezaki, E., *Thermal behavior of the hydrotalcite-like layered structure of Mg and Al-layered double hydroxides with interlayer carbonate by means of in situ powder HTXRD and DTA/TG.* Solid State Ionics, 1998. **106**(3–4): p. 279-284.

25. Kirkpatrick, R.J., *MAS NMR Spectroscopy of Minerals and Glasses* in *Spectroscopic Methods in Mineralogy and Geology*, F.C. Hawthorne, Editor. 1988, The Society. p. 341-403.

26. Andersen, M.D., H.J. Jakobsen, and J. Skibsted, *A new aluminium-hydrate species in hydrated Portland cements characterized by ^{27}Al and ^{29}Si MAS NMR spectroscopy.* Cement and Concrete Research, 2006. **36**(1): p. 3-17.

27. Andersen, M.D., H.J. Jakobsen, and J. Skibsted, *Incorporation of aluminum in the calcium silicate hydrate (C−S−H) of hydrated Portland cements: A high-field ^{27}Al and ^{29}Si MAS NMR investigation.* Inorganic Chemistry, 2003. **42**(7): p. 2280-2287.

28. Myers, R.J., et al., *The role of Al in cross-linking of alkali-activated slag cements.* Journal of the American Ceramic Society, 2015. **98**(3): p. 996-1004.

29. Sun, G.K., J.F. Young, and R.J. Kirkpatrick, *The role of Al in C-S-H: NMR, XRD, and compositional results for precipitated samples.* Cement and Concrete Research, 2006. **36**(1): p. 18-29.

30. Faucon, P., et al., *Aluminum incorporation in calcium silicate hydrates (C-S-H) depending on their Ca/Si ratio.* Journal of Physical Chemistry B, 1999. **103**(37): p. 7796-7802.

31. Pardal, X., et al., *^{27}Al and ^{29}Si solid-state NMR characterization of calcium-aluminosilicate-hydrate.* Inorganic Chemistry, 2012. **51**(3): p. 1827-1836.

32. Richardson, I.G., et al., *Location of aluminum in substituted calcium silicate hydrate (C-S-H) gels as determined by ^{29}Si and ^{27}Al NMR and EELS.* Journal of the American Ceramic Society, 1993. **76**(9): p. 2285-2288.

33. Famy, C., K.L. Scrivener, and A.K. Crumbie, *What causes differences of C-S-H gel grey levels in backscattered electron images?* Cement and Concrete Research, 2002. **32**(9): p. 1465-1471.

34. Bernal, S.A., et al., *High-resolution X-ray diffraction and fluorescence microscopy characterization of alkali-activated slag-metakaolin binders.* Journal of the American Ceramic Society, 2013. **96**(6): p. 1951-1957.

35. Ben Haha, M., et al., *Influence of activator type on hydration kinetics, hydrate assemblage and microstructural development of alkali activated blast-furnace slags.* Cement and Concrete Research, 2011. **41**(3): p. 301-310.

36. San Nicolas, R., et al., *Distinctive microstructural features of aged sodium silicate-activated slag concretes.* Cement and Concrete Research, 2014. **65**: p. 41-51.

37. Richardson, I.G., *The nature of C-S-H in hardened cements.* Cement and Concrete Research, 1999. **29**: p. 1131-1147.

38. Taylor, R., I.G. Richardson, and R.M.D. Brydson, *Composition and microstructure of 20-year-old ordinary Portland cement–ground granulated blast-furnace slag blends containing 0 to 100% slag.* Cement and Concrete Research, 2010. **40**(7): p. 971-983.

39. Arakcheeva, A.V., et al., *Crystal structure and comparative crystal chemistry of $Al_2Mg_4(OH)_{12}(CO_3) \cdot 3H_2O$, a new mineral from the hydrotalcite-manasseite group.* Krystallografiya, 1996: p. 1024-1034.

40. Wang, S.D., K.L. Scrivener, and P.L. Pratt, *Factors affecting the strength of alkali-activated slag.* Cement and Concrete Research, 1994. **24**(6): p. 1033-1043.